



Published in final edited form as:

*Radiother Oncol.* 2023 September ; 186: 109741. doi:10.1016/j.radonc.2023.109741.

## Ultra-High Dose-Rate Proton FLASH Improves Tumor Control

Samriddhi Shukla<sup>1</sup>, Taniya Saha<sup>1</sup>, Nihar Rama<sup>1</sup>, Anusha Acharya<sup>1</sup>, Tien Le<sup>1</sup>, Fenghua Bian<sup>1</sup>, Johnny Donovan<sup>1</sup>, Lin Abigail Tan<sup>1</sup>, Ralph Vatner<sup>4</sup>, Vladimir Kalinichenko<sup>1,2,3</sup>, Anthony Mascia<sup>4</sup>, John P Perentesis<sup>5</sup>, Tanya V Kalin<sup>1,2,#</sup>

<sup>1</sup>Divisions of Pulmonary Biology, Perinatal Institute of Cincinnati Children's Hospital Medical Center, 3333 Burnet Ave., Cincinnati, OH 45229

<sup>2</sup>Neonatology, Perinatal Institute of Cincinnati Children's Hospital Medical Center, 3333 Burnet Ave., Cincinnati, OH 45229

<sup>3</sup>Center for Lung Regenerative Medicine, Perinatal Institute of Cincinnati Children's Hospital Medical Center, 3333 Burnet Ave., Cincinnati, OH 45229

<sup>4</sup>Department of Radiation Oncology, University of Cincinnati College of Medicine, Cincinnati, OH, USA. Cincinnati Children's Hospital Medical Center, Cincinnati, OH, USA.

<sup>5</sup>Cincinnati Children's Hospital Medical Center, Division of Oncology Division of Experimental Hematology, Division of Biomedical Informatics, Cincinnati, OH 45229, USA

### Abstract

**Background and purpose**—Proton radiotherapy (PRT) offers potential benefits over other radiation modalities, including photon and electron radiotherapy. Increasing the rate at which radiation is delivered may provide a therapeutic advantage. Here, we compared the efficacy of conventional proton therapy (CONV<sup>Pt</sup>) to ultrahigh dose-rate proton therapy, FLASH<sup>Pt</sup>, in a mouse model of non-small cell lung cancers (NSCLC).

**Materials and methods**—Mice bearing orthotopic lung tumors received thoracic radiation therapy using CONV<sup>Pt</sup> (<0.05 Gy/s) and FLASH<sup>Pt</sup> (>60 Gy/s) dose rates.

**Results**—Compared to CONV<sup>Pt</sup>, FLASH<sup>Pt</sup> was more effective in reducing tumor burden and decreasing tumor cell proliferation. Furthermore, FLASH<sup>Pt</sup> was more efficient in increasing the infiltration of cytotoxic CD8<sup>+</sup> T-lymphocytes inside the tumor while simultaneously reducing the percentage of immunosuppressive regulatory T-cells (Tregs) among T-lymphocytes. Also, compared to CONV<sup>Pt</sup>, FLASH<sup>Pt</sup> was more effective in decreasing pro-tumorigenic M2-like macrophages in lung tumors, while increasing infiltration of anti-tumor M1-like macrophages. Finally, FLASH<sup>Pt</sup> treatment reduced expression of checkpoint inhibitors in lung tumors, indicating reduced immune tolerance.

#Corresponding author: Tanya V. Kalin, Cincinnati Children's Hospital Medical Center, 3333 Burnet Avenue, MLC 7009, Cincinnati, OH 45229-3039, Phone: (513) 803-1201, tatiana.kalin@cchmc.org.

**Publisher's Disclaimer:** This is a PDF file of an unedited manuscript that has been accepted for publication. As a service to our customers we are providing this early version of the manuscript. The manuscript will undergo copyediting, typesetting, and review of the resulting proof before it is published in its final form. Please note that during the production process errors may be discovered which could affect the content, and all legal disclaimers that apply to the journal pertain.

**Conclusions**—Our results suggest that FLASH dose-rate proton delivery modulates the immune system to improve tumor control and might thus be a promising new alternative to conventional dose rates for NSCLC treatment.

---

## Introduction

The goal of radiation therapy (RT) is to reduce or eliminate tumor burden while sparing normal tissues from long-term injury<sup>1</sup>. The recent developments in imaging technologies, treatment planning and delivery techniques have allowed highly conformal treatments to target the tumor at the highest possible dose of radiation while sparing normal tissue as much as possible. Although, these approaches significantly reduce the volume of normal tissue irradiated with high doses, the volume of normal tissue receiving low doses are increased. With the longer cancer-free survival in radiation-treated patients, the need to prevent the long-term complications resulting from normal tissue injury is still one of the main priorities in the field. Another important unmet clinical need is the development of tumor radiation resistance. Since some of solid tumors can be resistant to conventional radiotherapy, a different radiotherapeutic strategy is required for these patients.

Radiation therapy can be classified according to the types of radiation particles or waves that are used to deliver the treatment, such as photons, electrons, or protons. Photons and electrons are the most used radiations, based mainly on broader availability and more affordable technologies to generate photon and electron beams compared to protons. However, there are some limitations to these approaches. Photons deposit their radiation doses close to their entrance into the body, and they also have the exit dose downstream from the tumor, which increases the exposed normal surrounding tissue area and causes later complications. Electrons release most of their energy near the surface of the skin and are often used to treat superficial tumors, such as skin cancers and some lymph nodes. The electron radiation does not penetrate the skin far, preventing injury of the deeper normal tissues. However, electron radiotherapy cannot be used to treat the deeper tumors.

For patients who present with inoperable, locally advanced non-small lung cancers (NSCLC), photon-based RT remains the standard of care<sup>2</sup>. However, since lung tissue is highly sensitive to radiation, thoracic radiation using photon beams presents a unique challenge. The NSCLC treatments, including intensity-modulated radiation therapy (IMRT) and stereotactic body radiation therapy (SBRT), are still limited by toxicity to normal tissues, including acute esophagitis and subacute presentations of other pulmonary complications such as pneumonitis and pulmonary fibrosis<sup>3-8</sup>. In addition, most chemotherapeutic agents used in conjunction with photon radiotherapy increase the risk of damage to normal tissue. These dose-limiting toxicities of photon radiation have increased clinical interest in the emerging use of proton radiotherapy. Due to the unique dose absorption profile in tissue, known as the Bragg peak, proton beams deposit most of the destructive energy within the tumor target<sup>9-11</sup>. The release of proton energy can be precisely controlled, which minimizes the damage to the surrounding normal tissue in front and back of the tumor. In patients with non-small cell lung cancer (NSCLC), proton-beam therapy may enable safe dose escalation while sparing chest organs at risk and simultaneously maintaining adequate target coverage<sup>12,13</sup>.

Other efforts to reduce radiation-induced normal tissue toxicity and to maximize therapeutic efficacy of radiotherapy have been focusing on the dose rates at which radiation is delivered. Ultra-high dose-rate delivery of radiation, called FLASH radiotherapy, is garnering interest to improve the therapeutic ratio of radiation and to decrease normal tissue toxicity<sup>14-16</sup>. FLASH radiotherapy involves radiation delivery at a dose rate of 40 Gy/s, over thousand times higher than conventional RT used for clinical treatment, typically delivered at <0.05 Gy/s<sup>15,17</sup>. FLASH radiotherapy effects have been shown using electron beams delivered by experimental linear accelerators (LINACs) specifically constructed to deliver pulsed electron beam irradiation at ultra-high dose rates<sup>14,18</sup>. Electron FLASH (FLASH<sup>e</sup>) radiation has been reported to reduce normal tissue toxicity both *in vitro* and *in vivo* compared to equivalent doses of conventional dose-rate radiation<sup>17</sup>, suggesting that FLASH RT could be employed to facilitate dose escalation and reduce the incidence of radiation-mediated toxicities<sup>17</sup>. While FLASH<sup>e</sup> has shown promise to decrease the normal tissue toxicity and improve efficacy of tumor eradication<sup>19</sup>, the efficacy of proton FLASH (FLASH<sup>Pf</sup>) radiotherapy for anti-cancer therapy has been under investigated. The goal of the present study is to assess the efficacy of FLASH<sup>Pf</sup> on tumor control using a syngeneic orthotopic mouse model of NSCLC. To achieve this goal, FLASH<sup>Pf</sup> (dose rate 60 Gy/s) and CONV<sup>Pf</sup> (dose rate 1 Gy/s) were delivered to lung tumors using the clinical pencil beam scanning proton system. Our current study demonstrated that FLASH<sup>Pf</sup> is more effective than conventional proton therapy (CONV<sup>Pf</sup>) in decreasing the number of proliferating tumor cells and increasing recruitment of anti-tumor immune cells.

## Materials and Methods

### Orthotopic Lewis Lung Carcinoma (LLC) tumor model.

C57BL/6 mice (8-9 weeks old) were purchased from Jackson Lab (Bar Harbor, Maine). LLC-mCherry tumor cells (20,000 cells) were injected into the left lung lobe of C57BL/6 mice as described<sup>20</sup>. Tissues were harvested on day 20 and day 23 post tumor inoculation. Lung tumor sizes were measured using callipers. For calliper measurements, the tumor volume was calculated using the formula:  $V = \frac{1}{2} * L * W^2$  (L=Length, W=Width of the tumor). Equations were derived as previously described<sup>21</sup>.

### Pencil beam spot scanning delivery system and Proton radiation.

The proton therapy system includes a cyclotron with a maximum energy of 250MeV, a beam transport system, and rotating 360-degree gantry with a beam delivery nozzle equipped with a pencil beam scanning (PBS) system. The absolute dose was calibrated using an Advanced Markus ionization chamber (PTW Dosimetry, Germany) and Dose 1 electrometer (IBA Dosimetry, Germany). Both the ion chamber and electrometer were calibrated by National Institute of Standards and Technology (NIST) traceable absolute dose laboratory. The absolute dose was calculated using the IAEA TRS398 dose-to-water formulism ([http://www-naweb.iaea.org/nahu/dmrp/documents/cop\\_v12\\_2006-06-05.pdf](http://www-naweb.iaea.org/nahu/dmrp/documents/cop_v12_2006-06-05.pdf)). This methodology has been independently validated for conventional and FLASH dose and dose rates<sup>22,23</sup>. The irradiation conditions were single energy, transmission proton fields. The conventional dose rate, defined as 1 Gy/s, was a 244MeV single layer transmission beam. The FLASH dose rate field, defined at 60 Gy/s, was a 250MeV single layer transmission beam. Both the

conventional and FLASH fields were calibrated, using the above methodology, to give 18 Gy of physical proton dose. The field sizes were custom designed to cover both mouse lungs and spare the normal tissues. No collimators were used. Treatment plans were generated in the Eclipse™ treatment planning system (Varian Medical Systems, Palo Alto, CA) using in-house software and scripting. On day 15 post LLC tumor inoculation, the mice were anesthetized using room air/isoflurane anesthesia and immobilized on an in-house designed small animal platform and holder. While under anesthesia, the bi-lateral lungs of the tumor bearing mice were irradiated according to the above dose schemas. As a real-time quality assurance constancy check, the dose distal to the mouse was measured. For the conventional fields, the average dose and dose rate are 17.8Gy  $\pm$  0.07Gy and 0.9Gy/s  $\pm$  0.1Gy/s. For the FLASH fields, the average dose and dose rate are 18.1Gy  $\pm$  0.05Gy and 61.9Gy/s  $\pm$  2.0Gy/s. The acceptable dose tolerance of 3% and dose rate tolerance of 5% were all met.

### Histology and Immunostaining.

Frozen sections (8-10  $\mu$ m) of tumor bearing lungs were used for histology and immunohistochemical staining. Immunofluorescence staining was performed as described before<sup>24,25</sup>. Sections were blocked in 4% donkey serum and incubated with primary antibodies at 4°C overnight. Antibodies used: Goat polyclonal anti-Discosoma tdTomato (LSBio, CAT#C340696, dilution 1:100), Rabbit monoclonal anti- $\gamma$ H2A.X (Cell Signaling, CAT#9718, dilution 1:300), Rabbit monoclonal anti-Ki67 (Invitrogen, CAT#MA5-14520, dilution 1:200), Rat monoclonal anti-CD45 (BD Biosciences, CAT#553076 dilution 1:50), Goat polyclonal anti-CD3 (Santa Cruz, CAT#SC-1127, dilution 1:200), Rat monoclonal anti-CD4 (Invitrogen, CAT#4SM95, dilution 1:100), Rabbit polyclonal anti-CD8 alpha (Invitrogen, CAT#PA5-81344, dilution 1:200), Rabbit polyclonal anti-FOXP3 (Novus Biologicals, CAT#NB100-39002, dilution 1:200), Rat monoclonal anti-F4/80 (Biolegend, CAT#122602, dilution 1:100), Rabbit monoclonal anti-CD163 (Abcam, CAT#ab182422, dilution 1:100), Rabbit monoclonal anti-iNOS (Abcam, CAT#ab178945, dilution 1:100), Rabbit monoclonal PD-1 (Abcam, CAT#ab214421, dilution 1:100) and Rabbit polyclonal PD-L1 (Invitrogen, CAT#PA5-20343, dilution 1:100). After incubation with primary antibody, slides were washed and incubated at room temperature with appropriate fluorophore-conjugated secondary antibodies, and counterstained with DAPI. Images were obtained using a Zeiss AxioPlan 2 microscope or Nikon NiE widefield microscope as described<sup>26</sup>.

**Image analysis.**—Images were quantified using either NIS Elements version 4.5 or particle analyser plugin of ImageJ as described<sup>27,28</sup>. Briefly, for ImageJ quantification, images were exported as high-resolution files. Further, ImageJ Particle Analyzer plugin was used for counting positive cells after colour thresholding of single-color images from each group, counting all positive cells in 1-5 different fields (one single field of view represented the whole tumor in smaller tumors) from tumors of 3–8 mice/group, and calculating the average number of staining-positive cells. For NIS Elements image analyses, images were colour thresholded for each channel and then combined channels were used for quantifying staining-positive cells in the images. Data in graphs are presented as mean  $\pm$  SEM.

**Statistics:** Statistical analysis was performed using GraphPad Prism software v9 package (GraphPad Software, Inc., San Diego, CA, USA). Unpaired T-test with Welch's correction, Mann-Whitney log rank T test, and log-rank test corrected for multiple comparisons were used when and where appropriate.  $P < 0.05$  was considered significant and all tests were two-sided. Correlation analyses ( $r$ ) were performed by calculating Pearson correlation coefficients with 95% confidence intervals.

**Animal Study Approval.**—All animal studies were approved by Cincinnati Children's Research Foundation Institutional Animal Care and Use Committee and covered under our animal protocol (IACUC2022-0041). The Cincinnati Children's Research Foundation Institutional Animal Care and Use Committee is an AAALAC and NIH accredited institution (NIH Insurance #8310801). All mice were kept under SPF (specific-pathogen free) conditions in 12/12 light/dark cycle, 18–23 °C and 40–60% humidity. Both males and females were used for studies.

## Results

To compare anti-tumor effects of FLASH<sup>Pr</sup> and CONV<sup>Pr</sup> therapies, we used a previously established orthotopic mouse model of NSCLC in which mCherry-labelled Lewis Lung Carcinoma (LLC-mCherry) cells were injected into the left lung lobe. Two weeks after tumor cell inoculation, mice were randomly divided into groups and treated with a single fraction of 18 Gy proton radiation delivered to the bilateral thorax using 2 different modalities: (1) conventional dose rate delivering 1 Gy/s and (2) FLASH dose rate delivering 60 Gy/s. Mice were sacrificed and lungs were harvested day 5 and day 8 post radiation (Fig. 1A). Both CONV<sup>Pr</sup> and FLASH<sup>Pr</sup> treatments significantly reduced lung tumor volume compared to tumor volume in control mice at day 5 and day 8. No significant differences were observed between the volumes of CONV<sup>Pr</sup>- and FLASH<sup>Pr</sup>-treated tumors (Fig. 1B-D and Supplemental Fig. 1A-D). However, immunofluorescence staining of tumor sections showed significantly reduced number of mCherry-labelled tumor cells in FLASH<sup>Pr</sup>-treated tumors at both time points (Fig. 1E-F and Supplemental Fig. 2). These results demonstrate that FLASH<sup>Pr</sup> improves eradication of NSCLC tumor cells compared to CONV<sup>Pr</sup> treatment.

The observed reduction in the number of mCherry-labelled tumor cells within FLASH<sup>Pr</sup>-treated tumors led us to perform further histopathological analyses of radiated lung tumors. Proliferation of mCherry-labelled LLC tumor cells were assessed by Ki-67 staining. Both types of proton therapies effectively inhibited proliferation of tumor cells at both day 5 and day 8 post radiation compared to untreated control (Fig. 2A-B). At day 8, tumors from FLASH<sup>Pr</sup> group had significantly lower numbers of Ki67-positive tumor cells compared to the CONV<sup>Pr</sup> group (Fig. 2A-B). FLASH<sup>Pr</sup> group had also significantly higher percentage of apoptotic tumor cells compared to the CONV<sup>Pr</sup> group at both days 5 and 8 after proton irradiation treatment (Supplemental Fig. 3A-B). Since formation of  $\gamma$ H2A.X foci is a direct indicator of radiation damage to tumor cells, we performed  $\gamma$ H2A.X staining in the LLC tumors. The FLASH<sup>Pr</sup>-irradiated tumors had higher percentage of  $\gamma$ H2A.X positive tumor cells compared to CONV<sup>Pr</sup>-irradiated tumors at both day 5 and day 8 post radiation (Fig. 2C-D). To identify what other cell types contributed to the tumor volume, we performed immunostaining with CD45 antibody. We showed that the tumor mass in FLASH<sup>Pr</sup>-treated

group comprised mostly of CD45+ immune cells (Fig. 2E). The ratio of immune cells to tumor cells was higher in FLASH<sup>Pr</sup>-treated tumors compared to control and CONV<sup>Pr</sup>-irradiated tumors at day 5 and day 8 (Fig. 2E-F). Altogether, FLASH<sup>Pr</sup> treatment decreased proliferation of tumor cells, increased DNA damage of lung tumor cells and increased recruitment of CD45+ immune cells compared to CONV<sup>Pr</sup> treatment.

Previous studies demonstrated that T-cell infiltration into the tumor core is a positive predictor of response to radiation therapy<sup>29-31</sup>. Therefore, we examined the distribution of T-cells within the tumor using immunostaining for CD3, a marker of T-lymphocytes. In our mouse model of lung adenocarcinoma, in the untreated tumors, T-cells preferentially located around the tumor edge, with the tumor themselves being devoid of T-cells, an attribute of “immune-excluded” tumors (Figure 3A and 3C, top left panels). In response to CONV<sup>Pr</sup> and FLASH<sup>Pr</sup> treatments, the number of T-cells within the tumor was increased at both timepoints, with higher infiltration of CD3<sup>+</sup> T-cells in FLASH<sup>Pr</sup>-treated tumors (Fig. 3A and 3C). As a result, the number of T-lymphocytes FLASH<sup>Pr</sup>-treated tumors was dramatically increased compared to CONV<sup>Pr</sup> and untreated groups (Fig. 3B and D).

Since we observed an increased number of infiltrated CD3<sup>+</sup> T-cells within the proton-irradiated lung tumors (Fig. 3), we next explored which subtype of T-cells accounts for this increase. We used cell surface markers CD8 to identify cytotoxic T-cells, CD4 to identify T helper cells and FOXP3 to identify Tregs among CD3<sup>+</sup> lymphocytes at day 5 and day 8 after radiation treatment (Fig. 4A, Fig. 4E and Supplemental Fig. 3A). FLASH<sup>Pr</sup> treatment increased the proportion of CD8<sup>+</sup> T-cells but decreased the proportion of CD4<sup>+</sup> cells among total CD3<sup>+</sup> T-cells compared to untreated control or CONV<sup>Pr</sup> treated tumors at day 5 after treatment (Fig. 4B-C). At day 8 after irradiation, the FLASH<sup>Pr</sup>-treated tumors continued to have increased ratio of CD8<sup>+</sup> T-cells and decreased ratio of CD4<sup>+</sup> T-cells among CD3<sup>+</sup> T-cells compared to untreated control (Fig. 4D-F). Also, FLASH<sup>Pr</sup> irradiation increased the infiltration distance of CD8<sup>+</sup> T-cells compared to CONV<sup>Pr</sup>, indicating increased CD8<sup>+</sup> T-cell motility from the invasive edge into the tumor core at both day 5 and day 8 (Supplemental Fig. 4A). Furthermore, FLASH<sup>Pr</sup> radiation but not CONV<sup>Pr</sup> radiation decreased the percentage of Tregs among tumor-associated CD3<sup>+</sup> T-cells at both time points after treatment (Fig. 4G-I). Altogether, FLASH<sup>Pr</sup> treatment was more effective than CONV<sup>Pr</sup> irradiation in recruiting cytotoxic CD8<sup>+</sup> T-cell into the tumors and decreasing the recruitment of immunosuppressive Treg cells.

Since it has been shown that macrophages can regulate infiltration of CD8<sup>+</sup> cytotoxic T-cells into lung tumors<sup>32</sup>, we next focused on macrophages. We demonstrated that both CONV<sup>Pr</sup> and FLASH<sup>Pr</sup> treatments significantly reduced the number of F4/80<sup>+</sup> macrophages in lung tumors (Fig. 5A-B and Supplemental Fig. 4B-C). Moreover, FLASH<sup>Pr</sup>-treatment increased the ratio of CD8<sup>+</sup> T-cells to F4/80<sup>+</sup> macrophages within the tumor compared to untreated or CONV<sup>Pr</sup>-treated tumors at day 8 (Fig. 5C-D and Supplemental Fig. 4D-E).

Previous studies have shown that tumor-associated macrophages are heterogeneous, with pro-tumor M2-like macrophages expressing cell surface marker CD163<sup>33,34,35</sup>, whereas antitumor M1-like macrophages expressing inducible nitric oxide synthase (iNOS)<sup>36,37</sup>. In our model, the immunostaining with anti-CD163 antibodies was decreased in both

proton-treated groups (Supplemental Fig. 5A). The reduction in CD163<sup>+</sup> macrophages was positively correlated with the decreased number of mCherry<sup>+</sup> tumor cells (Supplemental Fig. 5A-B). Conversely, immunostaining with anti-iNOS antibody was increased in both irradiated groups (Supplemental Fig. 5C). The increase in the number of iNOS-positive cells was inversely correlated with the number of mCherry<sup>+</sup> tumor cells (Supplemental Fig. 5C-D).

Since the crosstalk between macrophages and T-cells were shown to be important for tumor progression<sup>32,38</sup>, we next assessed the connection between the distribution of macrophages and CD3<sup>+</sup> T-cells. Differential count of T-cells and macrophages within control and proton-irradiated tumors demonstrated that the number of tumor-associated CD3<sup>+</sup> T-cells negatively correlated with the number of CD163<sup>+</sup> M2-like macrophages (Fig. 5E-F and Supplemental Fig. 6A) and positively correlated with iNOS<sup>+</sup> M1-like macrophages (Fig. 5G-H and Supplemental Fig. 6B). Thus, macrophage polarization towards M1-like phenotype is conducive in increasing lymphocyte infiltration in lung tumors.

The activation of PD-1/PD-L1 pathway is a tumor adaptive immune resistance mechanism. PD-L1 is mainly expressed on tumor cells and its binding to PD-1 receptors on T-cells leads to the inactivation of cytotoxic activity of T-cells. FLASH<sup>Pt</sup> treatment decreased the percentage of PD1-positive CD3<sup>+</sup> T-lymphocytes at day 8 compared to untreated group (Fig. 6A-B and Supplemental Fig. 7A-B). Further, we observed significant reduction in PD-L1 expression on tumor cells in both CONV<sup>Pt</sup> and FLASH<sup>Pt</sup> groups with significantly higher PD-L1 reduction in FLASH<sup>Pt</sup> groups at both day 5 and day 8 (Fig. 6C-D and Supplemental Fig. 7C-D). These results indicate that FLASH<sup>Pt</sup> not only increases the cytotoxic T-cell infiltration to the tumor core, but also reverses their immunosuppressive phenotype.

## Discussion

NSCLC remains a deadly disease with treatment options that often fail to prevent disease progression. In both early stage and locally advanced disease, radiation therapy is a mainstay treatment that improves overall survival for NSCLC patients<sup>2,39,40</sup>. Given the immunosuppressive microenvironment of the lung tumors, there has been considerable interest in finding ways to render these tumors sensitive to anti-tumor immune response. The current standard of care for non-resectable stage-III NSCLC tumors is concurrent chemoradiotherapy followed by neoadjuvant and adjuvant therapy. Immune checkpoint inhibitors, including pembrolizumab, atezolizumab, combination of nivolumab and ipilimumab, have demonstrated survival benefits in clinical trials of lung cancer. Radiation oncologists continue to find better approaches to deliver the best tumoricidal radiation doses to tumors while minimizing the radiation doses to adjacent normal tissues and organs. Proton therapy offers unique physical and biological advantages leading to reduced toxicity and equal or improved efficacy over other radiotherapeutic modalities<sup>41</sup>. The increasing clinical usage of proton radiotherapy is representative of efforts to mitigate radiation-related adverse events, which currently present a major barrier to effective treatment of NSCLC using X-rays<sup>42</sup>. Based on the studies using both X-ray and electron radiation treatments, the FLASH modality of radiation delivery is a promising approach to reduce the toxicity of normal tissues and to increase or maintain the efficacy

of treatment compared with conventional electron radiotherapy<sup>17,42-45</sup>. It was shown that electron FLASH irradiation decreased the incidents of radiation-induced pulmonary fibrosis by preserving the lung progenitor cells and decreasing senescence of normal lung tissue<sup>19</sup>. Recent research has shown that proton radiation increases immune infiltration of tumors in subcutaneous CT26 colon tumor model<sup>46</sup> and hepatocellular carcinoma model<sup>47</sup>. FLASH<sup>Pr</sup> RT spared memory impairment produced by CONV<sup>Pr</sup> therapy and induced comparable T lymphocyte recruitment in orthotopic glioma rat model<sup>48</sup>. We have also previously reported higher immune infiltration of NSCLC tumors post FLASH proton radiation under oxygen anaesthesia<sup>49</sup>. Here, we report that thoracic irradiation of mice with orthotopic, syngeneic lung tumors using FLASH proton radiotherapy results in improved tumor control and increased immune cell infiltration. We observed higher immune infiltration of cytotoxic T lymphocytes with reduced immunosuppression in FLASH<sup>Pr</sup>-radiated tumors compared to the CONV<sup>Pr</sup>-radiated lung tumors. This FLASH-mediated amelioration of immunosuppression in lung tumor microenvironment contributes to the improved therapeutic response by FLASH<sup>Pr</sup> at isodoses with CONV<sup>Pr</sup>.

We found that tumor-bearing mice treated with CONV<sup>Pr</sup> and FLASH<sup>Pr</sup> treatments had lower tumor burden than untreated control tumor bearing mice. Reduction in tumor burden after radiotherapy has been shown to be a prognostic factor for NSCLC patients, showing a positive association between tumor volume shrinkage and overall survival<sup>50</sup>. In our study, FLASH<sup>Pr</sup> RT also induced an enlarged, rounded morphology in tumor cells, which is common for cells that have become senescent<sup>51</sup>. We further observed reduction in tumor cell proliferation after FLASH<sup>Pr</sup> treatment. Senescence is a well-established barrier to cancer progression as this phenomenon prevents tumor cells from proliferating and secreting pro-tumorigenic growth factors<sup>52,53</sup>. While the molecular mechanisms by which FLASH<sup>Pr</sup> inhibits tumor cell proliferation remain unclear, DNA-damage agents can cause senescence in tumor cells<sup>54-56</sup>. FLASH<sup>Pr</sup>-mediated higher DNA damage could be the reason of reduced cell proliferation in FLASH<sup>Pr</sup>-treated tumors.

The role of immune cells in modulating innate tumor progression or regression in response to therapy has been widely examined. The most striking developments were made in the field of immunotherapies to reactivate the immune systems of patients with a variety of cancer types, including NSCLC. The immune checkpoint inhibitors are emerging immunotherapies, but only elicit responses in a subset of patients. This has been attributed at least in part to the inability of T-cells to be effectively recruited to the tumor core<sup>57-59</sup>. Radiotherapy has been investigated in combination with immune checkpoint inhibitors in both preclinical experiments and multiple clinical trials, showing convincing evidence of synergistic effects from concurrent administration of immunotherapy and radiotherapy<sup>60-62</sup>. An important contribution of the present study is that delivery of protons with FLASH dose rates is more efficient in augmenting CD8<sup>+</sup> cytotoxic T-cell accumulation in the tumor core than conventional mode of RT delivery. We also show that the FLASH modes of proton RT decrease in the number of M2-like macrophages at the tumor edge. Since it was previously demonstrated that in squamous-cell carcinomas macrophages impede CD8<sup>+</sup> T-cells from reaching tumor cells<sup>56</sup>, we can speculate that FLASH increases CD8<sup>+</sup> T-cell trafficking into the tumor, probably due to the decrease in the number of M2-like macrophages at the tumor edge. In a recent study, single high-dose abdomino-pelvic FLASH<sup>e</sup> irradiation

was shown to maintain tumor control in a preclinical mouse model of ovarian cancer by enhancing the efficacy of PD-1 therapy and higher recruitment of cytotoxic CD8<sup>+</sup> T cells into the tumor <sup>63</sup>. It is possible that FLASH proton therapy can improve the efficacy of immune checkpoint inhibitors in NSCLC patients by increasing the recruitment of T-cells into tumors. Interestingly, we also observed downregulation of checkpoint inhibitory PD-1/PD-L1 signaling by FLASH<sup>Pr</sup> treatment.

One of the limitations of our study is that we have not tested several tumor cell lines with different immunogenic properties in FLASH radiation treatments. Such experiments can provide valuable information regarding the molecular mechanisms through which FLASH activates anti-tumor immune responses. Another limitation of our study is that some tumor cells after proton irradiation can lose the mCherry expression, making their identification by IF analysis difficult.

In summary, FLASH mode of proton RT demonstrates an efficient control of NSCLC tumors through immunomodulation. Compared to conventional dose-rate-delivered protons, FLASH proton radiotherapy reduces tumor burden, changes macrophage polarization towards the M1-like phenotype, increase CD8<sup>+</sup> T-cell infiltration into the tumor core and alters the tumor microenvironment towards a less immunotolerant one. The FLASH proton therapies represent promising new alternatives to conventional proton treatment.

## Supplementary Material

Refer to Web version on PubMed Central for supplementary material.

## Acknowledgement

This study was supported by the Varian funds (TVK, JPP) and by the NIH grants R01 HL132849 (TVK), R01 HL158659 (TVK).

## References

1. Graves PR, Siddiqui F, Anscher MS, Movsas B. Radiation pulmonary toxicity: from mechanisms to management. *Semin Radiat Oncol.* 2010;20(3):201–207. [PubMed: 20685583]
2. Ramella S, D'Angelillo RM. Proton beam or photon beam radiotherapy in the treatment of non-small-cell lung cancer. *Lancet Oncol.* 2020;21(7):873–875. [PubMed: 32615102]
3. Palma DA, Senan S, Tsujino K, et al. Predicting radiation pneumonitis after chemoradiation therapy for lung cancer: an international individual patient data meta-analysis. *Int J Radiat Oncol Biol Phys.* 2013;85(2):444–450. [PubMed: 22682812]
4. Lu C, Lei Z, Wu H, Lu H. Evaluating risk factors of radiation pneumonitis after stereotactic body radiation therapy in lung tumor: Meta-analysis of 9 observational studies. *PLoS One.* 2018;13(12):e0208637. [PubMed: 30521600]
5. Stauder MC, Macdonald OK, Olivier KR, et al. Early pulmonary toxicity following lung stereotactic body radiation therapy delivered in consecutive daily fractions. *Radiother Oncol.* 2011;99(2):166–171. [PubMed: 21571384]
6. Menoux I, Antoni D, Mazzara C, et al. Radiation-induced lung toxicity predictors: Retrospective analysis of 90 patients treated with stereotactic body radiation therapy for stage I non-small-cell lung carcinoma. *Cancer Radiother.* 2020;24(2):120–127. [PubMed: 32173269]

7. Tian S, Switchenko JM, Buchwald ZS, et al. Lung Stereotactic Body Radiation Therapy and Concurrent Immunotherapy: A Multicenter Safety and Toxicity Analysis. *Int J Radiat Oncol Biol Phys.* 2020;108(1):304–313. [PubMed: 31982496]
8. Ricco A, Barlow S, Feng J, et al. Repeat Thoracic Stereotactic Body Radiation Therapy (SBRT) for Nonsmall Cell Lung Cancer: Long-Term Outcomes, Toxicity, and Dosimetric Considerations. *Adv Radiat Oncol.* 2020;5(5):984–993. [PubMed: 33083662]
9. Higgins KA, O'Connell K, Liu Y, et al. National Cancer Database Analysis of Proton Versus Photon Radiation Therapy in Non-Small Cell Lung Cancer. *Int J Radiat Oncol Biol Phys.* 2017;97(1):128–137. [PubMed: 27979443]
10. van Marlen P, Dahele M, Folkerts M, Abel E, Slotman BJ, Verbakel W. Bringing FLASH to the Clinic: Treatment Planning Considerations for Ultrahigh Dose-Rate Proton Beams. *Int J Radiat Oncol Biol Phys.* 2020;106(3):621–629. [PubMed: 31759074]
11. Harada H, Murayama S. Proton beam therapy in non-small cell lung cancer: state of the art. *Lung Cancer (Auckl).* 2017;8:141–145. [PubMed: 28883747]
12. Verma V, Chang JY. Dose-escalation of locally advanced non-small cell lung cancer with proton beam therapy. *Transl Lung Cancer Res.* 2018;7(Suppl 3):S280–S282. [PubMed: 30393622]
13. Jie AW, Marignol L. Pro-con of proton: Dosimetric advantages of intensity-modulation over passive scatter for thoracic malignancies. *Tech Innov Patient Support Radiat Oncol.* 2020;15:37–46. [PubMed: 32954018]
14. Vozenin MC, Hendry JH, Limoli CL. Biological Benefits of Ultra-high Dose Rate FLASH Radiotherapy: Sleeping Beauty Awoken. *Clin Oncol (R Coll Radiol).* 2019;31(7):407–415. [PubMed: 31010708]
15. de Kruijff RM. FLASH radiotherapy: ultra-high dose rates to spare healthy tissue. *Int J Radiat Biol.* 2020;96(4):419–423. [PubMed: 31829765]
16. Zhou S, Zheng D, Fan Q, et al. Minimum dose rate estimation for pulsed FLASH radiotherapy: A dimensional analysis. *Med Phys.* 2020;47(7):3243–3249. [PubMed: 32279337]
17. Favaudon V, Fouillade C, Vozenin MC. [Ultrahigh dose-rate, "flash" irradiation minimizes the side-effects of radiotherapy]. *Cancer Radiother.* 2015;19(6-7):526–531. [PubMed: 26277238]
18. Durante M, Brauer-Krisch E, Hill M. Faster and safer? FLASH ultra-high dose rate in radiotherapy. *Br J Radiol.* 2018;91(1082):20170628. [PubMed: 29172684]
19. Favaudon V, Caplier L, Monceau V, et al. Ultrahigh dose-rate FLASH irradiation increases the differential response between normal and tumor tissue in mice. *Sci Transl Med.* 2014;6(245):245ra293.
20. Milewski D, Balli D, Ustiyani V, et al. FOXM1 activates AGR2 and causes progression of lung adenomas into invasive mucinous adenocarcinomas. *PLoS Genet.* 2017;13(12):e1007097. [PubMed: 29267283]
21. Shukla S, Milewski D, Pradhan A, et al. The FOXM1 Inhibitor RCM-1 Decreases Carcinogenesis and Nuclear beta-Catenin. *Mol Cancer Ther.* 2019;18(7):1217–1229. [PubMed: 31040162]
22. Lee E, Lourenco AM, Speth J, et al. Ultrahigh dose rate pencil beam scanning proton dosimetry using ion chambers and a calorimeter in support of first in-human FLASH clinical trial. *Med Phys.* 2022;49(9):6171–6182. [PubMed: 35780318]
23. Lourenco A, Subiel A, Lee N, et al. Absolute dosimetry for FLASH proton pencil beam scanning radiotherapy. *Sci Rep.* 2023;13(1):2054. [PubMed: 36739297]
24. Donovan J, Deng Z, Bian F, et al. Improving anti-tumor efficacy of low-dose Vincristine in rhabdomyosarcoma via the combination therapy with FOXM1 inhibitor RCM1. *Front Oncol.* 2023;13:1112859. [PubMed: 36816948]
25. Milewski D, Pradhan A, Wang X, et al. FoxF1 and FoxF2 transcription factors synergistically promote rhabdomyosarcoma carcinogenesis by repressing transcription of p21(Cip1) CDK inhibitor. *Oncogene.* 2017;36(6):850–862. [PubMed: 27425595]
26. Milewski D, Shukla S, Gryder BE, et al. FOXF1 is required for the oncogenic properties of PAX3-FOXO1 in rhabdomyosarcoma. *Oncogene.* 2021;40(12):2182–2199. [PubMed: 33627785]
27. Black M, Arumugam P, Shukla S, et al. FOXM1 nuclear transcription factor translocates into mitochondria and inhibits oxidative phosphorylation. *Mol Biol Cell.* 2020;31(13):1411–1424. [PubMed: 32348194]

28. Balli D, Zhang Y, Snyder J, Kalinichenko VV, Kalin TV. Endothelial cell-specific deletion of transcription factor FoxM1 increases urethane-induced lung carcinogenesis. *Cancer Res.* 2011;71(1):40–50. [PubMed: 21199796]
29. Liu H, Zhang T, Ye J, et al. Tumor-infiltrating lymphocytes predict response to chemotherapy in patients with advanced non-small cell lung cancer. *Cancer Immunol Immunother.* 2012;61(10):1849–1856. [PubMed: 22456757]
30. Schulze AB, Evers G, Gorlich D, et al. Tumor infiltrating T cells influence prognosis in stage I-III non-small cell lung cancer. *J Thorac Dis.* 2020;12(5):1824–1842. [PubMed: 32642087]
31. Talebian Yazdi M, van Riet S, van Schadewijk A, et al. The positive prognostic effect of stromal CD8+ tumor-infiltrating T cells is restrained by the expression of HLA-E in non-small cell lung carcinoma. *Oncotarget.* 2016;7(3):3477–3488. [PubMed: 26658106]
32. Peranzoni E, Lemoine J, Vimeux L, et al. Macrophages impede CD8 T cells from reaching tumor cells and limit the efficacy of anti-PD-1 treatment. *Proc Natl Acad Sci U S A.* 2018;115(17):E4041–E4050. [PubMed: 29632196]
33. Balli D, Ren X, Chou FS, et al. Foxm1 transcription factor is required for macrophage migration during lung inflammation and tumor formation. *Oncogene.* 2012;31(34):3875–3888. [PubMed: 22139074]
34. Shiraishi D, Fujiwara Y, Horlad H, et al. CD163 Is Required for Protumoral Activation of Macrophages in Human and Murine Sarcoma. *Cancer Res.* 2018;78(12):3255–3266. [PubMed: 29610117]
35. Kubota K, Moriyama M, Furukawa S, et al. CD163<sup>(+)</sup>CD204<sup>(+)</sup> tumor-associated macrophages contribute to T cell regulation via interleukin-10 and PD-L1 production in oral squamous cell carcinoma. *Sci Rep.* 2017;7(1):1755. [PubMed: 28496107]
36. Paul S, Chhatar S, Mishra A, Lal G. Natural killer T cell activation increases iNOS<sup>(+)</sup>CD206<sup>(-)</sup> M1 macrophage and controls the growth of solid tumor. *J Immunother Cancer.* 2019;7(1):208. [PubMed: 31387637]
37. Sun L, Kees T, Almeida AS, et al. Activating a collaborative innate-adaptive immune response to control metastasis. *Cancer Cell.* 2021;39(10):1361–1374 e1369. [PubMed: 34478639]
38. Singhal S, Stadanlick J, Annunziata MJ, et al. Human tumor-associated monocytes/macrophages and their regulation of T cell responses in early-stage lung cancer. *Sci Transl Med.* 2019;11(479).
39. Safi S, Beckhove P, Warth A, et al. A randomized phase II study of radiation induced immune boost in operable non-small cell lung cancer (RadImmune trial). *BMC Cancer.* 2015;15:988. [PubMed: 26686362]
40. Cheng M, Jolly S, Quarshie WO, Kapadia N, Vigneau FD, Kong FS. Modern Radiation Further Improves Survival in Non-Small Cell Lung Cancer: An Analysis of 288,670 Patients. *J Cancer.* 2019;10(1):168–177. [PubMed: 30662537]
41. Alexander M, Kim SY, Cheng H. Update 2020: Management of Non-Small Cell Lung Cancer. *Lung.* 2020;198(6):897–907. [PubMed: 33175991]
42. Eling L, Bouchet A, Nemoz C, et al. Ultra high dose rate Synchrotron Microbeam Radiation Therapy. Preclinical evidence in view of a clinical transfer. *Radiother Oncol.* 2019;139:56–61. [PubMed: 31307824]
43. Zhu H, Xie D, Wang Y, et al. Comparison of intratumor and local immune response between MV X-ray FLASH and conventional radiotherapies. *Clin Transl Radiat Oncol.* 2023;38:138–146. [PubMed: 36425537]
44. Allen BD, Alaghband Y, Kramar EA, et al. Elucidating the neurological mechanism of the FLASH effect in juvenile mice exposed to hypofractionated radiotherapy. *Neuro Oncol.* 2022.
45. Shi X, Yang Y, Zhang W, et al. FLASH X-ray spares intestinal crypts from pyroptosis initiated by cGAS-STING activation upon radioimmunotherapy. *Proc Natl Acad Sci U S A.* 2022;119(43):e2208506119. [PubMed: 36256824]
46. Mirjolet C, Nicol A, Limagne E, et al. Impact of proton therapy on antitumor immune response. *Sci Rep.* 2021;11(1):13444. [PubMed: 34188135]
47. Chen MF, Chen PT, Hsieh CC, Wang CC. Effect of Proton Therapy on Tumor Cell Killing and Immune Microenvironment for Hepatocellular Carcinoma. *Cells.* 2023;12(2).

48. Iturri L, Bertho A, Lamirault C, et al. Proton FLASH Radiation Therapy and Immune Infiltration: Evaluation in an Orthotopic Glioma Rat Model. *Int J Radiat Oncol Biol Phys*. 2022.
49. Rama NS T; Shukla S; Goda C; Milewski D; Mascia AE; Vatner RE; Sengupta D; Katsis A; Abel E; Girdhani S; Miyazaki M; Rodriguez A; Ku A; Dua R; Parry R; Kalin TV . Improved Tumor Control Through T-cell Infiltration Modulated by Ultra-High Dose Rate Proton FLASH Using a Clinical Pencil Beam Scanning Proton System. *International Journal of Radiation Oncology\*Biography\*Physics*. 2019;105(1):164–165.
50. Takenaka T, Yamazaki K, Miura N, Mori R, Takeo S. The Prognostic Impact of Tumor Volume in Patients with Clinical Stage IA Non-Small Cell Lung Cancer. *J Thorac Oncol*. 2016;11(7):1074–1080. [PubMed: 26899756]
51. Sikora E, Mosieniak G, Sliwinska MA. Morphological and Functional Characteristic of Senescent Cancer Cells. *Curr Drug Targets*. 2016;17(4):377–387. [PubMed: 26477465]
52. Schosserer M, Grillari J, Breitenbach M. The Dual Role of Cellular Senescence in Developing Tumors and Their Response to Cancer Therapy. *Front Oncol*. 2017;7:278. [PubMed: 29218300]
53. Lee M, Lee JS. Exploiting tumor cell senescence in anticancer therapy. *BMB Rep*. 2014;47(2):51–59. [PubMed: 24411464]
54. Baar MP, Brandt RMC, Putavet DA, et al. Targeted Apoptosis of Senescent Cells Restores Tissue Homeostasis in Response to Chemotoxicity and Aging. *Cell*. 2017;169(1):132–147 e116. [PubMed: 28340339]
55. Shao L, Feng W, Li H, et al. Total body irradiation causes long-term mouse BM injury via induction of HSC premature senescence in an Ink4a- and Arf-independent manner. *Blood*. 2014;123(20):3105–3115. [PubMed: 24622326]
56. Liao EC, Hsu YT, Chuah QY, et al. Radiation induces senescence and a bystander effect through metabolic alterations. *Cell Death Dis*. 2014;5:e1255. [PubMed: 24853433]
57. Fares CM, Van Allen EM, Drake CG, Allison JP, Hu-Lieskovan S. Mechanisms of Resistance to Immune Checkpoint Blockade: Why Does Checkpoint Inhibitor Immunotherapy Not Work for All Patients? *Am Soc Clin Oncol Educ Book*. 2019;39:147–164. [PubMed: 31099674]
58. Jenkins RW, Barbie DA, Flaherty KT. Mechanisms of resistance to immune checkpoint inhibitors. *Br J Cancer*. 2018;118(1):9–16. [PubMed: 29319049]
59. Kalbasi A, Ribas A. Tumour-intrinsic resistance to immune checkpoint blockade. *Nat Rev Immunol*. 2020;20(1):25–39. [PubMed: 31570880]
60. Ko EC, Raben D, Formenti SC. The Integration of Radiotherapy with Immunotherapy for the Treatment of Non-Small Cell Lung Cancer. *Clin Cancer Res*. 2018;24(23):5792–5806. [PubMed: 29945993]
61. Formenti SC, Rudqvist NP, Golden E, et al. Radiotherapy induces responses of lung cancer to CTLA-4 blockade. *Nat Med*. 2018;24(12):1845–1851. [PubMed: 30397353]
62. Herter-Sprie GS, Koyama S, Korideck H, et al. Synergy of radiotherapy and PD-1 blockade in Kras-mutant lung cancer. *JCI Insight*. 2016;1(9):e87415. [PubMed: 27699275]
63. Eggold JT, Chow S, Melemenidis S, et al. Abdominopelvic FLASH Irradiation Improves PD-1 Immune Checkpoint Inhibition in Preclinical Models of Ovarian Cancer. *Mol Cancer Ther*. 2022;21(2):371–381. [PubMed: 34866044]

**Highlights:**

- FLASH<sup>PF</sup> radiation is more efficient to eliminate tumor cells compared to conventional proton radiation.
- FLASH<sup>PF</sup> radiation increases infiltration of cytotoxic CD8<sup>+</sup> T lymphocytes and decreases number of immunosuppressive Tregs compared to conventional radiation.
- FLASH<sup>PF</sup> radiation decreases expression of PD1/PD-L1 markers in lung tumors.

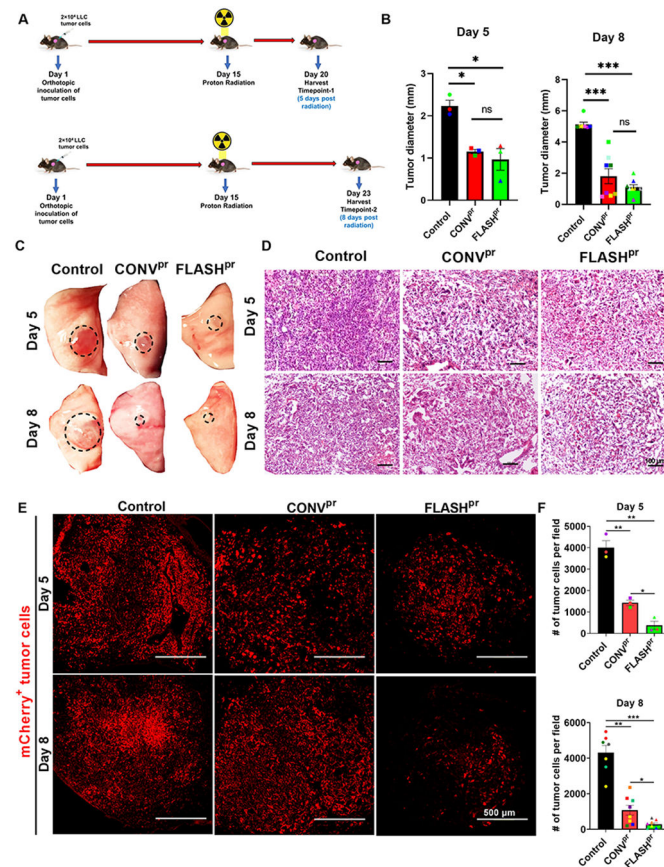


**Figure 1. FLASH<sup>Pr</sup> has better efficacy in reducing lung tumor burden compared to CONV<sup>Pr</sup>.** (A) Experimental schematic for LLC orthotopic model of lung cancer, and timeline of irradiation and tissue harvest. (B) Mice treated with FLASH<sup>Pr</sup> and CONV<sup>Pr</sup> radiation have decreased lung tumor diameters compared to control tumor bearing mice. Tumors were measured using calipers at day 5 (3 mice per group) and day 8 (8 mice per group). (C) Representative images of tumor-bearing left lung lobe from each group at day 5 and day 8 post radiation. (D) Representative images after H&E staining of lung tumors at day 5 and day 8. (Scale bar 100  $\mu$ m). (E-F) Immunofluorescence staining for mCherry-labelled tumor cells shows significant reduction of tumor burden at day 5 and day 8 in FLASH<sup>Pr</sup> group compared to control and CONV<sup>Pr</sup>. (Scale bar 500  $\mu$ m). \*, P<0.05; \*\*, P<0.01; \*\*\*, P<0.001.

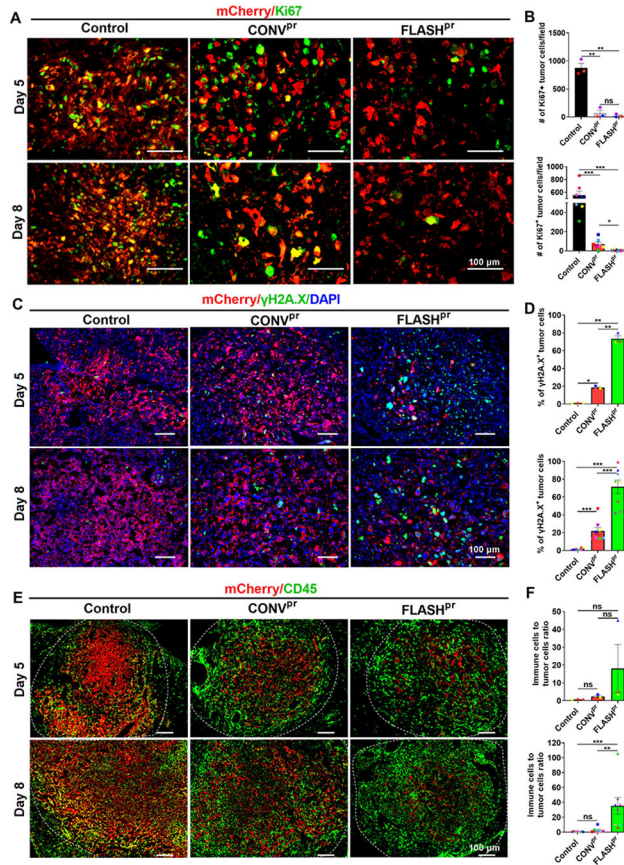


**Figure 2. FLASH decreases the number of proliferating tumor cells compared to conventional dose-rate proton treatment.**

(A-B) Number of Ki67 positive tumor cells is decreased in lung tumors treated with FLASH<sup>Pt</sup> compared to CONV<sup>Pt</sup>. Number of mCherry and Ki67 double positive cells per field was counted for each tumor and presented as average ± SEM (Scale bar 100 μm). Each dot represents one biological replicate. (C-D) FLASH<sup>Pt</sup> increases the percentage of mCherry/γH2A.X-double positive tumor cells compared to CONV<sup>Pt</sup>. Nuclei are counterstained with DAPI. Percentage of double positive cells were calculated for each tumor and presented as mean percentage ± SEM (Scale bar 100 μm). Each dot represents one biological replicate. (E-F) FLASH<sup>Pt</sup> increases the CD45<sup>+</sup> immune cells to mCherry<sup>+</sup> tumor cell ratio in lung tumors. Number of mCherry<sup>+</sup> tumor cells and CD45<sup>+</sup> immune cells were counted for each tumor and presented as the mean ratio of immune cells to tumor cells ± SEM (Scale bar 100 μm). Each dot represents one biological replicate. N = 3-8 mice per group; \*, P<0.05; \*\*, P<0.01; \*\*\*, P<0.001.

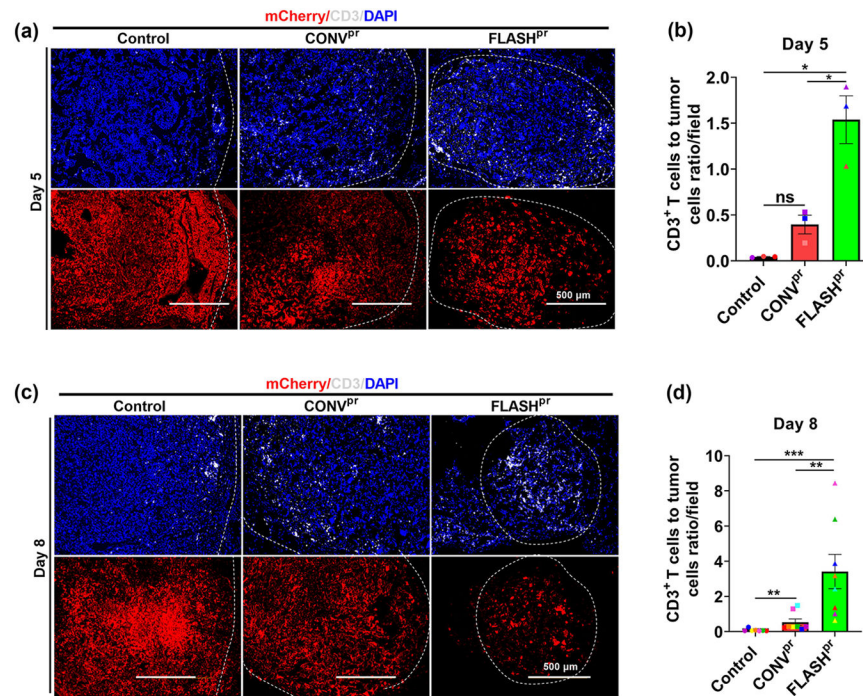


**Figure 3. FLASH proton irradiation increase infiltration of CD3<sup>+</sup> T-cells into tumors.** (A-B) Immunostaining with anti-CD3 antibody shows increased ratio between the number of T-lymphocytes and tumor cells in FLASH<sup>Pr</sup>-treated mice compared to CONV<sup>Pr</sup> at day 5 post radiation. The lower panel shows corresponding mCherry-positive tumor. Each dot represents the number of CD3<sup>+</sup> T-cells/field for one biological replicate and data is presented as group mean  $\pm$  SEM. N=3 mice per group (Scale bar 500  $\mu$ m). (C-D) FLASH<sup>Pr</sup> increases the ratio of T-cells to tumor cells at day 8 after irradiation. Each dot represents the ratio of CD3<sup>+</sup> T-cells to tumor cells for one biological replicate and data is presented as group mean  $\pm$  SEM. (Scale bar 500  $\mu$ m). N=8 mice per group. \*, P<0.05; \*\*, P<0.01; \*\*\*, P<0.001.

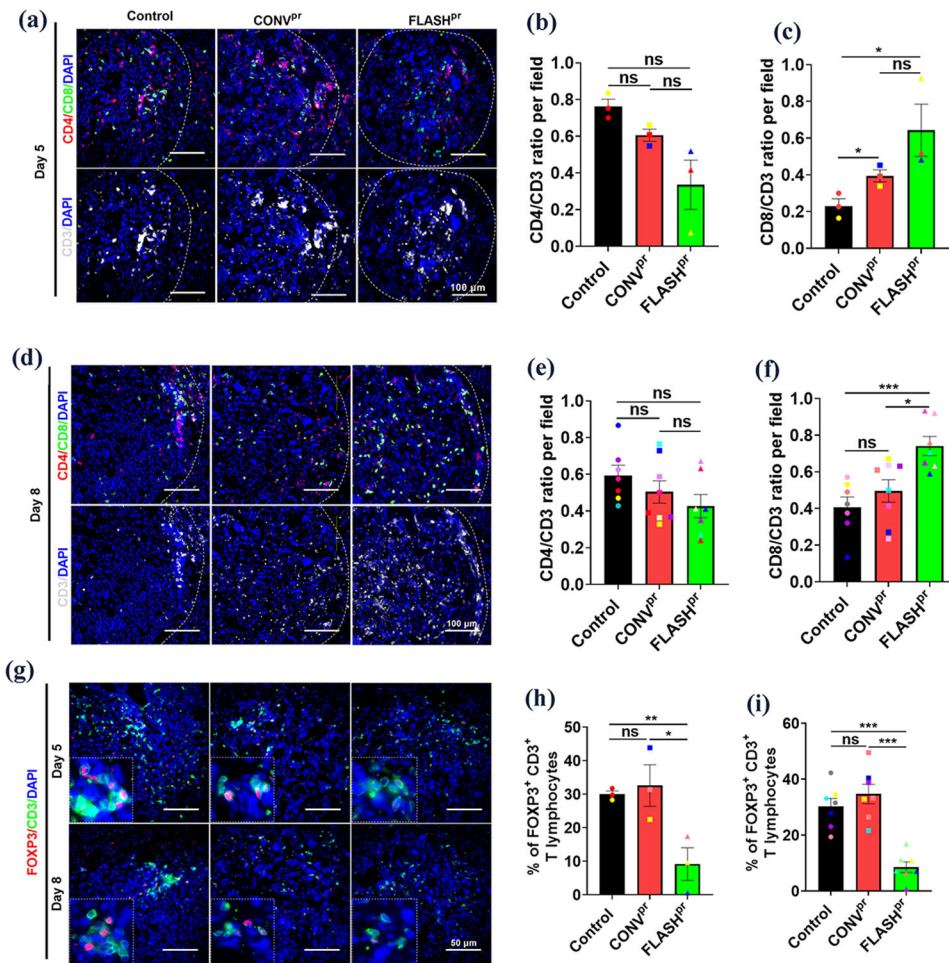


**Figure 4. FLASH<sup>Pr</sup> increases infiltration of CD8<sup>+</sup> cytotoxic T-cell into the tumor and reduces the number of Tregs.**

(A-C) Co-localization studies show the distribution of CD3<sup>+</sup> T-cells (white), CD4<sup>+</sup> helper T-cells (red) and CD8<sup>+</sup> cytotoxic T-cells (green) inside lung tumors of different treatment groups at day 5 post radiation. Average numbers of CD4<sup>+</sup>, CD8<sup>+</sup> and CD3<sup>+</sup> T-lymphocytes in the lung tumors of different treatment groups were calculated for each biological replicate and presented as mean ratio  $\pm$  SEM (Scale bar 100  $\mu$ m). N=3 per group. (D-F) Co-localization studies show the distribution of CD4<sup>+</sup> helper T-cells (red) and CD8<sup>+</sup> cytotoxic T-cells (green) inside lung tumors of different treatment groups at day 8 post radiation. Average numbers of CD4<sup>+</sup>, CD8<sup>+</sup> and CD3<sup>+</sup> T-lymphocytes in the lung tumors of different treatment groups were calculated for each biological replicate and presented as mean ratio  $\pm$  SEM (Scale bar 100  $\mu$ m). N=8 per group. (G-I) Co-localization studies show the distribution of FOXP3<sup>+</sup> Tregs (red) among CD3<sup>+</sup> T-lymphocytes (green) inside lung tumors of different proton-irradiated groups at day 5 and day 8 (Scale bar 50  $\mu$ m). Graph shows the percentage of FOXP3<sup>+</sup> Tregs among total tumor associated CD3<sup>+</sup> T-lymphocytes. Percentage of FOXP3<sup>+</sup> Tregs for each biological replicate was counted and presented as mean  $\pm$  SEM. N=3-8 per group. \*, P<0.05; \*\*, P<0.01; \*\*\*, P<0.001.

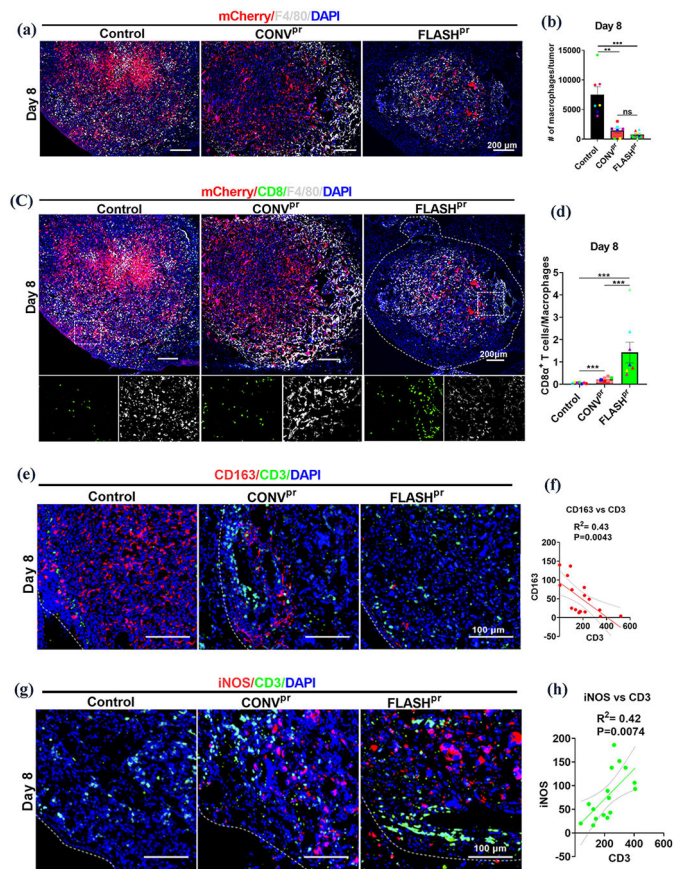


**Figure 5. FLASH<sup>Pf</sup> reduces the number of macrophages and increases the infiltration of T cells in tumors.**

(A-B) Representative images show distribution of F4/80<sup>+</sup> macrophages (white) in proton-treated and untreated lung tumors at day 8. LLC tumor cells are shown in red and nuclei are counterstained with DAPI (Scale bar 200  $\mu$ m). Number of mCherry<sup>+</sup> tumor cells and F4/80<sup>+</sup> macrophages were counted for each biological replicate and presented as the ratio of macrophages to tumor cells per field  $\pm$  SEM. (C-D) Co-localization studies show the distribution of CD8<sup>+</sup> cytotoxic T-cells (green) and F4/80<sup>+</sup> tumor-associated macrophages (white) among the mCherry-labelled tumor cells (red) in lung tumors of different treatment groups at day 8 (Scale bar 200  $\mu$ m). Inserts are 20X images showing CD8<sup>+</sup> cytotoxic T cells (green) and F4/80<sup>+</sup> tumor-associated macrophages (white). Graphs show the ratio of CD8<sup>+</sup> T-lymphocytes to F4/80<sup>+</sup> macrophages per tumor. Data is representative of complete tumor fields and presented as mean ratio  $\pm$  SEM. N= 8 per group. \*, P<0.05; \*\*, P<0.01; \*\*\*, P<0.001. (E-F) Co-localization studies demonstrate the decrease in the number of CD163<sup>+</sup> cells (red) and the increase in the number of CD3<sup>+</sup> T-lymphocytes (green) in the irradiated lung tumors compared to untreated tumors. Representative images of CD3<sup>+</sup> T-cells and CD163<sup>+</sup> cells at day 8 (Scale bar 100  $\mu$ m). Graph shows correlation between the numbers of CD3<sup>+</sup> T-cells and CD163<sup>+</sup> M2-like macrophages in lung tumors. (G-H) Co-localization studies demonstrate the increase in the number of iNOS<sup>+</sup> cells (red) and the increase in the number of CD3<sup>+</sup> T-lymphocytes (green) in the radiation-treated lung tumors compared to untreated tumors. Representative images of CD3<sup>+</sup> T-cells and iNOS<sup>+</sup> cells distribution at day

8 (Scale bar 100  $\mu\text{m}$ ). Graph shows correlation between the number of CD3<sup>+</sup> T-cells and iNOS<sup>+</sup> M1-like macrophages in the lung tumors.

Author Manuscript

Author Manuscript

Author Manuscript

Author Manuscript

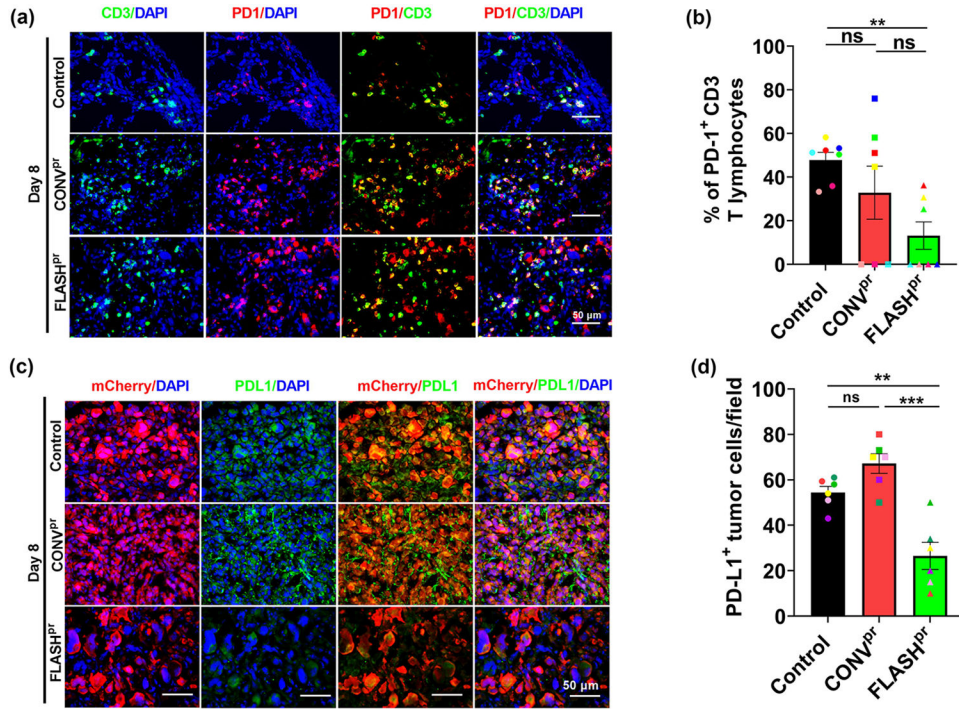


**Figure 6. FLASH<sup>P</sup> inhibits expression of checkpoint inhibitors PD-1 and PD-L1.** (A-B) Co-localization studies show the expression of PD-1 (red) among CD3<sup>+</sup> T-lymphocytes (green) in lung tumors of different treatment groups at day 8 (Scale bar 50 μm). Nuclei were counterstained with DAPI. At least five tumors per group were used to calculate percentage of PD-1<sup>+</sup> T-lymphocytes and presented as mean ratio ± SEM. N=5-7 per group. \*, P<0.05; \*\*, P<0.01; \*\*\*, P<0.001. (C-D) Co-localization studies show the expression of PD-L1 (green) among lung tumor cells (red) in different treatment groups at day 8 (Scale bar 50 μm). Nuclei were counterstained with DAPI. At least five tumors per group were used to calculate percentage of PD-1<sup>+</sup> T-lymphocytes and presented as mean ratio ± SEM. \*, P<0.05; \*\*, P<0.01; \*\*\*, P<0.001.